Numerical Simulation of Ram Extrusion Process for Ceramic Materials

Mingyang Li[1], Lie Tang[1], Fei Xue[2], Robert Landers[1]

[1]Missouri University of Science and Technology

[2]Shanghai Dianji University

REVIEWED, August 17 2011

Abstract

The freeze–form extrusion process for aqueous–based ceramic paste is complex due to the non–Newtonian behavior of the paste. In this paper the process is studied numerically using a developed mathematical model. The ceramic paste viscosity is characterized by the Herschel–Bulkley model. The relationship between plunger velocity and extrusion force is computed numerically. The influence of air, which is mixed with the paste during the loading process, is also examined. Due to the compressibility introduced by the trapped air, the plunger force dynamic response is typically dominated by a first order response. It is also shown that the extrusion plunger force depends on the volume of air in the extruder. Good agreement is obtained between the simulation results and experimental data.

Keywords: Ceramic paste extrusion; Numerical simulation; Non–Newtonian flow

Nomenclature

A :	Cross–sectional Area $\left(m^2\right)$
C, D :	Constants
F :	Force $\left(N\right)$
k :	Consistency index $\left(kg/m\cdot s\right)$
l :	Length $\left(m\right)$
n :	Power law index
p :	Pressure $\left(Pa\right)$
$\dot{p}$:	Pressure drop rate $\left(Pa/m\right)$
r,θ,z :	Coordinate $\left(m,rad,m\right)$
T :	Temperature $\left(K\right)$
t :	Time $\left(s\right)$
u_r,u_θ,u_z :	Velocity in r, θ and z directions $\left(m/s\right)$

u_{bulk}: Paste bulk velocity (m/s)

u_p: Plunger velocity (m/s)

V: Volume (m^3)

$\dot{V}$: Volume flow rate (m^3/s)

ρ: Density (kg/m^3)

η: Non–Newtonian viscosity $(Pa \cdot s)$

τ: Shear stress (Pa)

τ_0: Yield stress threshold (Pa)

γ: Shear rate (s^{-1})

γ_c: Critical shear rate (s^{-1})

1. Introduction

Due to their high heat resistance and hardness, ceramic materials are widely used in automotive, aerospace and other modern industries. However, traditional technologies for ceramic material processing are often expensive and time consuming, especially when complex geometries are involved. In recently years, several Solid Freeform Fabrication (SFF) processes have been developed to fabricate ceramic components from three–dimensional (3D) CAD models, including Fused Deposition of Ceramics [1], Fused Deposition Modeling [2], Extrusion Freeform Fabrication [3], 3D Printing [4], Selective Laser Sintering [5,6], Shape Deposition Manufacturing [7], and Robocasting [8, 9].

Freeze–form Extrusion Fabrication (FEF) is a novel, environmentally friendly SFF method for ceramic parts fabrication [10–12]. It is designed to use ceramic pastes with a high solids loading up to 50 vol.% and only trace amounts of organic binder (vol.1–4%). During the process, aqueous based colloidal paste is extruded from one or multiple extruders to fabricate a ceramic component in a layer–by–layer manner. The low temperature environment will help the part to maintain its shape by freezing the water present in the paste.

The behavior of the paste flow and the paste characteristics (e.g., viscosity and compressibility) are crucial for ceramic component fabrication using extrusion methods. During paste preparation and loading, air bubbles are trapped in the paste, resulting in paste compressibility. Paste compressibility has typically been ignored by previous research studies concerning paste flow behavior and characteristics, e.g., Benbow–Bridgwater equation [13], viscoplasticity method [14], upper bound techniques [15], finite element method [16,17], and artificial neural network [18].

So far, few studies have been conducted in analysing the dynamic response of extrusion forces when extruding non Newtonian pastes. An analytical model is first developed to describe the relationship between plunger velocity and extrusion force when paste compressi1bility is considered. The simulation results are then compared with experimental results.

2. Geometry and Boundary Conditions

2.1 Geometry

A ram extruder for viscosity measurement is used to study the relationship between extrusion force and plunger velocity. As shown in Fig.1, the ram extruder includes a barrel (part 2) to hold the paste, a die (part 4) with a small diameter, a plunger (parts 5 and 7) and seals (parts 1, 3, and 6). The geometry model and symbols of the extruder are shown in Fig. 2.

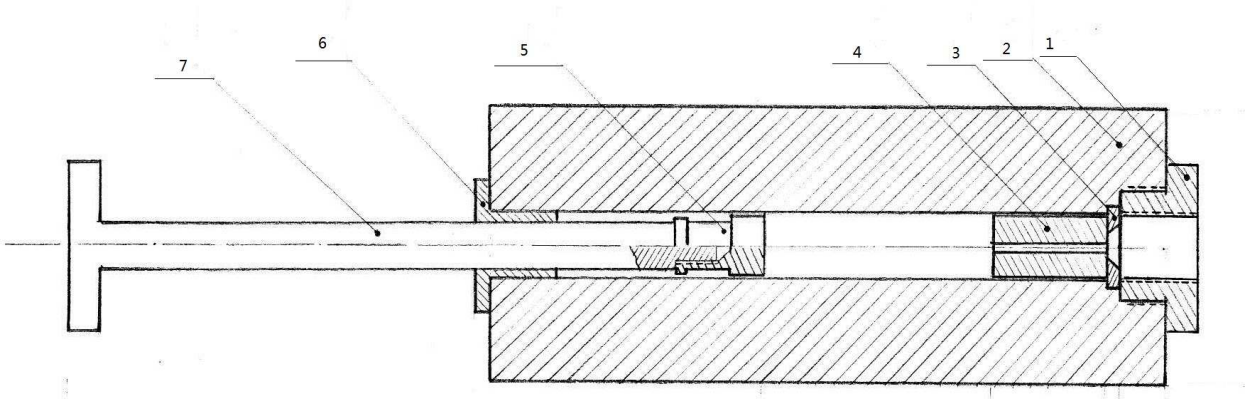

Fig. 1: Ram extruder schematic.

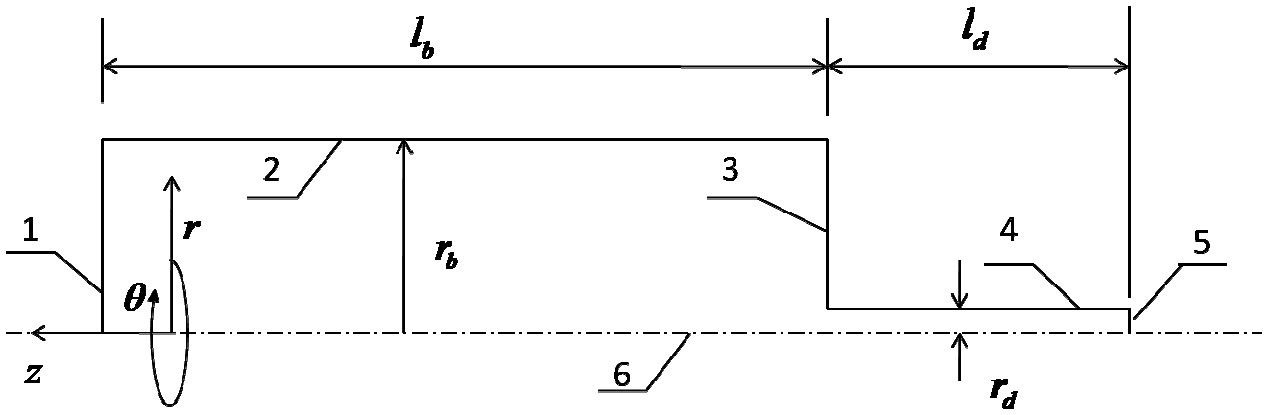

Fig. 2: Ram extruder model.

The dimensions of this ram extruder are $l_b = 60\ mm$, $l_d = 20\ mm$, and $r_b = 4.775\ mm$. Two different diameter dies, die 1 ($r_d = 0.548\ mm$) and die 2 ($r_d = 1.048\ mm$), are used in this study.

2.2 Assumptions

The following assumptions are made:

(1) Since the velocity is small and the viscosity is large, the Reynold Number will be small; therefore, the flow is taken as laminar.
(2) The material is homogenous.
(3) The barrel is completely filled by paste, except for studies where air is present.
(4) If otherwise stated, the paste is considered to be incompressible.
(5) The temperature is constant. Therefore, viscosity is only a function of shear rate and density is only a function of pressure.
(6) The paste does not experience slip at the wall.

2.3 Boundary Conditions

The following boundary conditions are used:

(1) Since the paste does not experience slip at the wall, the relative velocity of the paste at the wall in each direction is zero.
(2) The pressure at the extruder outlet is 101325 Pa. Therefore, the pressure of the paste at boundary 5 shown in Fig. 2 is 101325 Pa.
(3) The plunger is modeled as a moving wall. Thus, the velocity of fluid at boundary 1 shown in Fig. 2 is equal to u_p.

3. Mathematical Modeling

3.1 Governing equations

For paste flowing in a pipe, its continuity and momentum equations are given by the Navier–Stokes equations in cylindrical coordinates. Since there is no source or velocity in the θ direction, the terms involve θ can be neglected. The continuity equation becomes

$$\frac{1}{r}\frac{\partial}{\partial r}\left(ru_r\right)+\frac{\partial u_z}{\partial z}=0 \tag{1}$$

The momentum equation in the radial direction becomes

$$\rho\left[\frac{\partial u_r}{\partial t}+u_r\frac{\partial u_r}{\partial r}+u_z\frac{\partial u_z}{\partial z}\right]=\rho g_r-\frac{\partial p}{\partial r}+\frac{1}{r}\frac{\partial}{\partial r}\left(r\tau_{rr}\right)-\frac{\tau_{rr}}{r}+\frac{\partial \tau_{rz}}{\partial z} \tag{2}$$

The momentum equation in the θ direction is neglected and the momentum equation in the z direction becomes

$$\rho\left[\frac{\partial u_z}{\partial t}+u_r\frac{\partial u_z}{\partial r}+u_z\frac{\partial u_z}{\partial z}\right]=\rho g_z-\frac{\partial p}{\partial z}+\frac{1}{r}\frac{\partial}{\partial r}\left(r\tau_{rz}\right)+\frac{\partial \tau_{zz}}{\partial z} \tag{3}$$

3.2 Viscosity model

The paste viscosity is described by Herschel–Bulkley model [19]

$$\eta=\begin{cases}\dfrac{\tau_0}{\gamma}+k\left(\dfrac{\gamma}{\gamma_c}\right)^{n-1} & \text{if} \quad \gamma>\gamma_c \\ \left[\dfrac{2\tau_0}{\gamma_c}+k\left(2-n\right)\right]+\left[\dfrac{k\left(n-1\right)}{\gamma_c}-\dfrac{\tau_0}{\gamma_c^2}\right]\gamma & \text{if} \quad \gamma\le\gamma_c\end{cases} \tag{4}$$

3.3 Pressure drop rate

For fully developed flow, $\frac{\partial u_z}{\partial t}=0$, $u_r=0$, $\frac{\partial u_z}{\partial z}=0$, and $\frac{\partial \tau_{zz}}{\partial z}=0$. In this case equation (2) can be neglected, and equation (3) can be rewritten as

$$\rho g_z-\frac{\partial p}{\partial z}+\frac{1}{r}\frac{\partial}{\partial r}\left(r\tau_{rz}\right)=0 \tag{5}$$

Rearranging equation (5) and integrating with respect to r

$$r\tau_{rz}=\frac{1}{2}\left(\frac{\partial p}{\partial z}-\rho g_z\right)r^2+D_0 \tag{6}$$

When $r=0$, τ_{rz} must be finite. Therefore, $D_0=0$ and

$$\tau_{rz}=\frac{1}{2}\left(\frac{\partial p}{\partial z}-\rho g_z\right)r \tag{7}$$

When fluid flows in the negative z direction (i.e., $\frac{\partial u_z}{\partial r}>0$) the value of τ_{rz} should be positive. From equation (4) and using this fact

$$\tau_{rz} = \begin{cases} \tau_0 + \dfrac{k}{\gamma_c^{n-1}}\left(\dfrac{\partial u_z}{\partial r}\right)^n & \text{if} \quad \dfrac{\partial u_z}{\partial r} \geq \gamma_c \\ \left[\dfrac{2\tau_0}{\gamma_c} + k\left(2-n\right)\right]\left(\dfrac{\partial u_z}{\partial r}\right) + \left[\dfrac{k\left(n-1\right)}{\gamma_c} - \dfrac{\tau_0}{\gamma_c^2}\right]\left(\dfrac{\partial u_z}{\partial r}\right)^2 & \text{if} \quad \dfrac{\partial u_z}{\partial r} < \gamma_c \end{cases} \tag{8}$$

From equation (8), when $\dfrac{\partial u_z}{\partial r} \geq \gamma_c$

$$\tau_0 + \frac{k}{\gamma_c^{n-1}}\left(\frac{\partial u_z}{\partial r}\right)^n = \frac{1}{2}\left(\frac{\partial p}{\partial z} - \rho g_z\right) r \tag{9}$$

Rearranging equation (9)

$$\frac{\partial u_z}{\partial r} = \frac{du_z}{dr} = \left[\frac{\gamma_c^{n-1}\left(\dfrac{\partial p}{\partial z} - \rho g_z\right)}{2k} r - \frac{\gamma_c^{n-1}\tau_0}{k}\right]^{\frac{1}{n}} \tag{10}$$

Letting $\dot{p} = \left(\dfrac{\partial p}{\partial z} - \rho g_z\right)$, $C_1 = \dfrac{\gamma_c^{n-1}}{2k}$, and $C_2 = \dfrac{\gamma_c^{n-1}\tau_0}{k}$, equation (10) can be rewritten as

$$\frac{du_z}{dr} = \left(C_1 \dot{p} r - C_2\right)^{\frac{1}{n}} \tag{11}$$

Solving equation (11)

$$u_z = \frac{n}{n+1} \cdot \frac{1}{C_1 \dot{p}} \left(C_1 \dot{p} r - C_2\right)^{\frac{n+1}{n}} + D_1 \tag{12}$$

From equation (8) with $\dfrac{\partial u_z}{\partial r} < \gamma_c$

$$\left[\frac{2\tau_0}{\dot{\gamma}_c} + k\left(2-n\right)\right]\left(\frac{\partial u_z}{\partial r}\right) + \left[\frac{k\left(n-1\right)}{\gamma_c} - \frac{\tau_0}{\gamma_c^2}\right]\left(\frac{\partial u_z}{\partial r}\right)^2 = \frac{1}{2}\left(\frac{\partial p}{\partial z} - \rho g_z\right) r \tag{13}$$

Letting $C_3 = \dfrac{2\tau_0}{\gamma_c} + k\left(2-n\right)$ and $C_4 = \dfrac{k\left(n-1\right)}{\gamma_c} - \dfrac{\tau_0}{\gamma_c^2}$, equation (13) can be rewritten as

$$C_4\left(\frac{\partial u_z}{\partial r}\right)^2+C_3\left(\frac{\partial u_z}{\partial r}\right)-\frac{1}{2}\dot{p}r=0 \tag{14}$$

Solving equation (14)

$$\frac{\partial u_z}{\partial r}=\frac{du_z}{dr}=\frac{\pm\sqrt{C_3^2+2C_4\dot{p}r}-C_3}{2C_4}=\pm\frac{1}{2C_4}\left(C_3^2+2C_4\dot{p}r\right)^{\frac{1}{2}}-\frac{C_3}{2C_4} \tag{15}$$

Since $\tau_0>0$, $\gamma_c>0$, $k>0$, $\dot{p}>0$, $r\geq 0$, and $0<n<1$, $C_3>0$ and $C_4<0$. Therefore, if $\frac{du_z}{dr}=-\frac{1}{2C_4}\left(C_3^2+2C_4\dot{p}r\right)^{\frac{1}{2}}-\frac{C_3}{2C_4}$, when $r=0$

$$\frac{du_z}{dr}=-\frac{C_3}{C_4}=-\frac{\frac{2\tau_0}{\gamma_c}+k\left(2-n\right)}{\frac{k\left(n-1\right)}{\gamma_c}-\frac{\tau_0}{\gamma_c^2}}=\frac{2\tau_0+\gamma_c k\left(2-n\right)}{\tau_0+\gamma_c k\left(1-n\right)}\cdot\gamma_c>2\gamma_c \tag{16}$$

This is contrary to the assumption $\frac{\partial u_z}{\partial r}<\gamma_c$. Therefore

$$\frac{du_z}{dr}=\frac{1}{2C_4}\left(C_3^2+2C_4\dot{p}r\right)^{\frac{1}{2}}-\frac{C_3}{2C_4} \tag{17}$$

Solving equation (17)

$$u_z=\frac{1}{6C_4^2C_0}\left(C_3^2+2C_4\dot{p}r\right)^{\frac{3}{2}}-\frac{C_3}{2C_4}r+D_2 \tag{18}$$

Therefore, the paste velocity in the z direction is

$$u_z=\begin{cases}\dfrac{n}{n+1}\cdot\dfrac{1}{C_1\dot{p}}\left(C_1\dot{p}r-C_2\right)^{\frac{n+1}{n}}+D_1 & \text{if} \quad \dfrac{\partial u_z}{\partial r}\geq\gamma_c \\ \dfrac{1}{6C_4^2\dot{p}}\left(C_3^2+2C_4\dot{p}r\right)^{\frac{3}{2}}-\dfrac{C_3}{2C_4}r+D_2 & \text{if} \quad \dfrac{\partial u_z}{\partial r}<\gamma_c\end{cases} \tag{19}$$

There are two possible conditions at $r=r_0$: (1) $\frac{\partial u_z}{\partial r}\leq\gamma_c$ and (2) $\frac{\partial u_z}{\partial r}>\gamma_c$. For condition (1), the governing equations are

$$u_z = \frac{1}{6C_4^2\dot{p}}\left(C_3^2 + 2C_4\dot{p}r\right)^{\frac{3}{2}} - \frac{C_3}{2C_4}r + D_2 \tag{20}$$

$$\int_A u_z dA = 2\pi\int_0^{r_0} u_z r dr = \dot{V} = \pi r_0^2 u_{bulk} \tag{21}$$

The boundary condition is

$$u_z\big|_{r=r_0} = 0 \tag{22}$$

Substituting equation (22) into equation (20)

$$0 = \frac{1}{6C_4^2\dot{p}}\left(C_3^2 + 2C_4\dot{p}r_0\right)^{\frac{3}{2}} - \frac{C_3}{2C_4}r_0 + D_2 \tag{23}$$

Solving equation (23) for D_2

$$D_2 = \frac{C_3}{2C_4}r_0 - \frac{1}{6C_4^2\dot{p}}\left(C_3^2 + 2C_4\dot{p}r_0\right)^{\frac{3}{2}} \tag{24}$$

Substituting equation (24) into equation (20)

$$u_z = \left[\frac{1}{6C_4^2\dot{p}}\left(C_3^2 + 2C_4\dot{p}r\right)^{\frac{3}{2}} - \frac{C_3}{2C_4}r\right] - \left[\frac{1}{6C_4^2\dot{p}}\left(C_3^2 + 2C_4\dot{p}r_0\right)^{\frac{3}{2}} - \frac{C_3}{2C_4}r_0\right] \tag{25}$$

Substituting equation (25) into equation (21)

$$\int_0^{r_0}\left\{\left[\frac{1}{6C_4^2\dot{p}}\left(C_3^2 + 2C_4\dot{p}r\right)^{\frac{3}{2}} - \frac{C_3}{2C_4}r\right] - \left[\frac{1}{6C_4^2\dot{p}}\left(C_3^2 + 2C_4\dot{p}r_0\right)^{\frac{3}{2}} - \frac{C_3}{2C_4}r_0\right]\right\} r dr = \frac{u_{bulk}r_0^2}{2} \tag{26}$$

Integrating equation (26)

$$\frac{r_0\left(C_3^2 + 2C_4\dot{p}r_0\right)^{\frac{5}{2}}}{30C_4^3\dot{p}^2} + \frac{C_3^7 - \left(C_3^2 + 2C_4\dot{p}r_0\right)^{\frac{7}{2}}}{210C_4^4\dot{p}^3} + \frac{C_3 r_0^3}{12C_4} - \frac{\left(C_3^2 + 2C_4\dot{p}r_0\right)^{\frac{3}{2}} r_0^2}{12C_4^2\dot{p}} - \frac{u_{bulk}r_0^2}{2} = 0 \tag{27}$$

In equation (27), the parameters C_1, C_2, C_3, and C_4 are functions of the material property, and the parameter r_0 is determined by the ram geometry. Then, given a value for u_{bulk}, $\dot{p}$ can be computed numerically by equation (27). For condition (2), the governing equations are given by equation (21) and

$$u_z = \begin{cases} \dfrac{n}{n+1}\cdot\dfrac{1}{C_1\dot{p}}\left(C_1\dot{p}r - C_2\right)^{\frac{n+1}{n}} + D_1 & \text{if} \quad \dfrac{\partial u_z}{\partial r} \geq \gamma_c \\ \dfrac{1}{6C_4^2\dot{p}}\left(C_3^2 + 2C_4\dot{p}r\right)^{\frac{3}{2}} - \dfrac{C_3}{2C_4}r + D_2 & \text{if} \quad \dfrac{\partial u_z}{\partial r} < \gamma_c \end{cases} \tag{28}$$

The boundary conditions are given by equation (22) and when $\frac{\partial u_z}{\partial r} = \gamma_c$, u_z is continuous.

Substituting equation (21) into equation (28) for $\frac{\partial u_z}{\partial r} \geq \gamma_c$

$$\frac{n}{n+1}\cdot\frac{1}{C_1\dot{p}}\left(C_1\dot{p}r_0 - C_2\right)^{\frac{n+1}{n}} + D_1 = 0 \tag{29}$$

Solving equation (29) for D_1

$$D_1 = -\frac{n}{n+1}\cdot\frac{1}{C_1\dot{p}}\left(C_1\dot{p}r_0 - C_2\right)^{\frac{n+1}{n}} \tag{30}$$

Substituting equation (30) into equation (28) for $\frac{\partial u_z}{\partial r} \geq \gamma_c$

$$u_z = \frac{n}{n+1}\cdot\frac{1}{C_1\dot{p}}\left(C_1\dot{p}r - C_2\right)^{\frac{n+1}{n}} - \frac{n}{n+1}\cdot\frac{1}{C_1\dot{p}}\left(C_1\dot{p}r_0 - C_2\right)^{\frac{n+1}{n}} \tag{31}$$

Therefore, when $\frac{\partial u_z}{\partial r} = \gamma_c$, the radius at which the critical shear rate occurs is

$$r_c = \frac{\gamma_c^n + C_2}{C_1\dot{p}} \tag{32}$$

Since u_z is continuous when $\frac{\partial u_z}{\partial r} = \gamma_c$

$$\frac{n}{n+1}\cdot\frac{1}{C_1\dot{p}}\left[\left(C_1\dot{p}r_c - C_2\right)^{\frac{n+1}{n}} - \left(C_1\dot{p}r_0 - C_2\right)^{\frac{n+1}{n}}\right] = \frac{1}{6C_4^2\dot{p}}\left(C_3^2 + 2C_4\dot{p}r_c\right)^{\frac{3}{2}} - \frac{C_3}{2C_4}r_c + D_2 \tag{33}$$

Substituting equation (32) into equation (33)

$$D_2 = \frac{n}{n+1}\cdot\frac{1}{C_1\dot{p}}\left[\gamma_c^{n+1} - \left(C_1\dot{p}r_0 - C_2\right)^{\frac{n+1}{n}}\right] + \frac{C_3\left(\gamma_c^n + C_2\right)}{2C_4C_1\dot{p}} - \frac{1}{6C_4^2\dot{p}}\left[C_3^2 + \frac{2C_4\left(\gamma_c^n + C_2\right)}{C_1}\right]^{\frac{3}{2}} \tag{34}$$

Substituting equation (34) into equation (28) for $\frac{\partial u_z}{\partial r} < \gamma_c$

$$u_z = \frac{1}{6C_4^2\dot{p}}\left(C_3^2 + 2C_4\dot{p}r\right)^{\frac{3}{2}} - \frac{C_3}{2C_4}r + \frac{n}{n+1}\cdot\frac{1}{C_1\dot{p}}\left[\gamma_c^{n+1} - \left(C_1\dot{p}r_0 - C_2\right)^{\frac{n+1}{n}}\right] + \frac{C_3\left(\gamma_c^n + C_2\right)}{2C_4C_1\dot{p}} - \frac{1}{6C_4^2\dot{p}}\left[C_3^2 + \frac{2C_4\left(\gamma_c^n + C_2\right)}{C_1}\right]^{\frac{3}{2}} \tag{35}$$

From equation (21)

$$\int_0^{r_0} u_z r dr = \int_0^{r_c} u_z r dr + \int_{r_c}^{r_0} u_z r dr = \frac{u_{bulk} r_0^2}{2} \tag{36}$$

Substituting equation (31) and (35) into equation (36)

$$\begin{aligned}
&\frac{\left(\gamma_c^n + C_2\right)\left[C_3^2 + \frac{2C_4\left(\gamma_c^n + C_2\right)}{C_1}\right]^{\frac{5}{2}}}{30C_4^3C_1\dot{p}^3} + \frac{C_3^7 - \left[C_3^2 + \frac{2C_4\left(\gamma_c^n + C_2\right)}{C_1}\right]^{\frac{7}{2}}}{210C_4^4\dot{p}^3} - \frac{C_3}{6C_4}\left(\frac{\gamma_c^n + C_2}{C_1\dot{p}}\right)^3 \\
&+ \frac{1}{2}\left\{\frac{n}{n+1}\cdot\frac{1}{C_1\dot{p}}\left[\gamma_c^{n+1} - \left(C_1\dot{p}r_0 - C_2\right)^{\frac{n+1}{n}}\right] + \frac{C_3\left(\gamma_c^n + C_2\right)}{2C_4C_1\dot{p}}\right. \\
&\left. - \frac{1}{6C_4^2\dot{p}}\left[C_3^2 + \frac{2C_4\left(\gamma_c^n + C_2\right)}{C_1}\right]^{\frac{3}{2}}\right\}\left(\frac{\gamma_c^n + C_2}{C_1\dot{p}}\right)^2 \\
&+ \frac{n^2}{(n+1)(2n+1)}\cdot\frac{1}{C_1^2\dot{p}^2}\left[r_0\left(C_1\dot{p}r_0 - C_2\right)^{\frac{2n+1}{n}} - \left(\frac{\gamma_c^n + C_2}{C_1\dot{p}}\right)\gamma_c^{2n+1}\right] \\
&- \frac{n^3}{(n+1)(2n+1)(3n+1)}\cdot\frac{1}{C_1^3\dot{p}^3}\left[\left(C_1\dot{p}r_0 - C_2\right)^{\frac{3n+1}{n}} - \gamma_c^{3n+1}\right] \\
&- \frac{n}{2(n+1)}\cdot\frac{1}{C_1\dot{p}}\left(C_1\dot{p}r_0 - C_2\right)^{\frac{n+1}{n}}\left[r_0^2 - \left(\frac{\gamma_c^n + C_2}{C_1\dot{p}}\right)^2\right] - \frac{u_{bulk}r_0^2}{2} \\
&= 0
\end{aligned} \tag{37}$$

In equation (37), γ_c, C_1, C_2, C_3, and C_4 are given or functions of material properties, and r_0 is determined by the ram geometry. Given a value of u_{bulk}, $\dot{p}$ can be solved numerically by

equation (37). Then, for a specific ram geometry and u_{bulk}, r_c is calculated from equation (32) and $\dot{p}$ is solved from equation (27) or equation (37).

3.4 Dynamic response

Consider a particle of compressible material in an incompressible paste. The mixture flows in a pipe, as shown in Fig. 3.

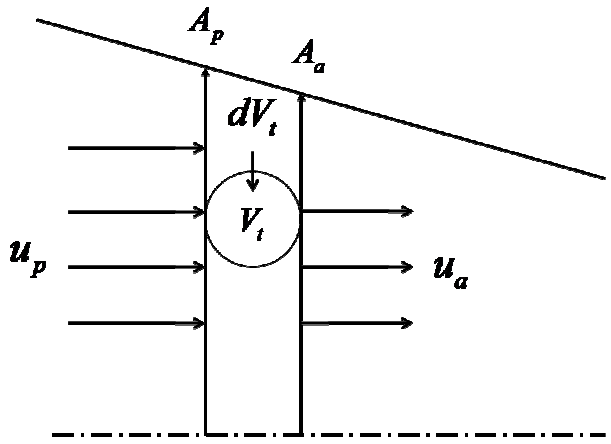

Fig. 3: Schematic of a particle of compressible material in an incompressible paste flowing in a pipe.

Applying mass conservation to the incompressible paste

$$\int_{A_a} u_a dA - \int_{A_p} u_p dA = \frac{dV(t)}{dt} \tag{38}$$

The volume of the particle of compressible material is a function of pressure

$$V = V(p_t) \tag{39}$$

From Section 3.3 and $p = \dot{p} l_d$

$$p = p(z, u_a) \tag{40}$$

When the ram geometry consists of a large radius barrel connected with a small radius needle, it can be shown that the pressure drop in the barrel can be neglected. This situation can be modeled as a layer of compressible material (either pure compressible material or a mixture of

compressible material and incompressible paste) above incompressible paste in the barrel. This situation is illustrated in Fig. 4.

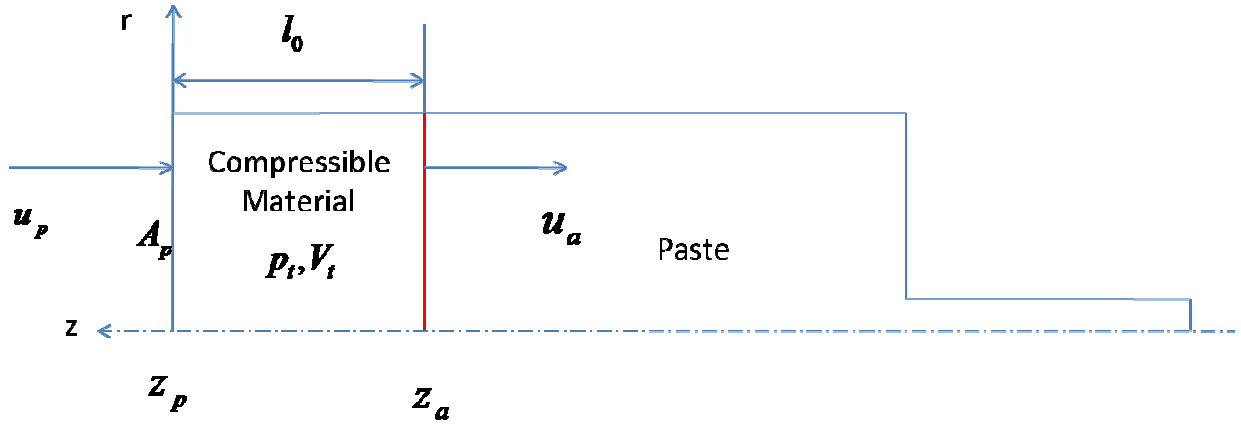

Fig. 4: Schematic of a situation with a layer of compressible material above incompressible paste in the barrel.

In this model, p is only a function of u_a. In this case, equations (38) and (40), respectively, can be written as

$$\left(u_a - u_p\right) A_p = \frac{dV\left(t\right)}{dt} \tag{41}$$

$$p = p\left(u_a\right) \tag{42}$$

If the compressible material in Fig. 4 is pure air with initial layer thickness l_0, equation (39) becomes

$$V\left(t\right) = \frac{p\left(0\right)V\left(0\right)}{p\left(t\right)} \tag{43}$$

Integrate equation (41) with respect to time and noting that $V\left(0\right) = l_0 A_p$

$$V\left(t\right) = \left[z_a - z_p\left(t\right)\right] A_p \tag{44}$$

Combining equations (43) and (44), and solving for $p\left(t\right)$

$$p\left(t\right) = \frac{p\left(0\right) l_0}{z_a - z_p\left(t\right)} \tag{45}$$

Substituting equation (45) into equation (42) with the expression $u_a = \frac{dz_a}{dt}$

$$p(t) = p\left(\frac{dz_a}{dt}\right) = \frac{p(0)l_0}{z_a - z_p(t)} \tag{46}$$

This equation can be rewritten as the following Initial Value Problem

$$\frac{dz_a}{dt} = p^{-1}\left[\frac{p(0)l_0}{z_a - z_p(t)}\right] \tag{47}$$

where $z_a(0) = l_0$. In this case, z_a can be obtained by solving equation (47), and u_a and F_{ram}, respectively, can be obtained from $u_a = \frac{dz_a}{dt}$ and $F_{ram} = p(u_a)A_p$.

4. Results and Discussion

In order to predict the extrusion force, a paste viscosity is obtained by conducting a set of experiments using die 1 (i.e., $r_d = 0.548$ *mm*). After determining the paste viscosity model, a series of experiments are conducted using die 2 ($r_d = 1.048$ *mm*) to validate the viscosity model. The dynamic response data is also recorded in these experiments.

Each experiment consists of three extrusion experiments, two without paste and one with paste. The first experiment is conducted without paste at a ram velocity 0.25 mm/s to test whether the barrel and plunger have been well lubricated. The second experiment is conducted without paste using the same ram velocity that will be used in the third experiment, which will be conducted with paste. The second experiment is used to determine the friction between the barrel and plunger.

4.1 Viscosity Model

The paste viscosity is tested using the ram extruder depicted in Fig. 1 with die 1. The Herschel–Bulkley model parameters are identified using steady state forces for different plunger velocities. The viscosity model parameters are listed in Table 1. The identified model is then compared with experimental results in Fig. 5. The goodness of fit is validated by a sum of squares due to the error of 2.78 N^2, a correlation coefficient of 0.993, and a root mean squared error of 1.18 N.

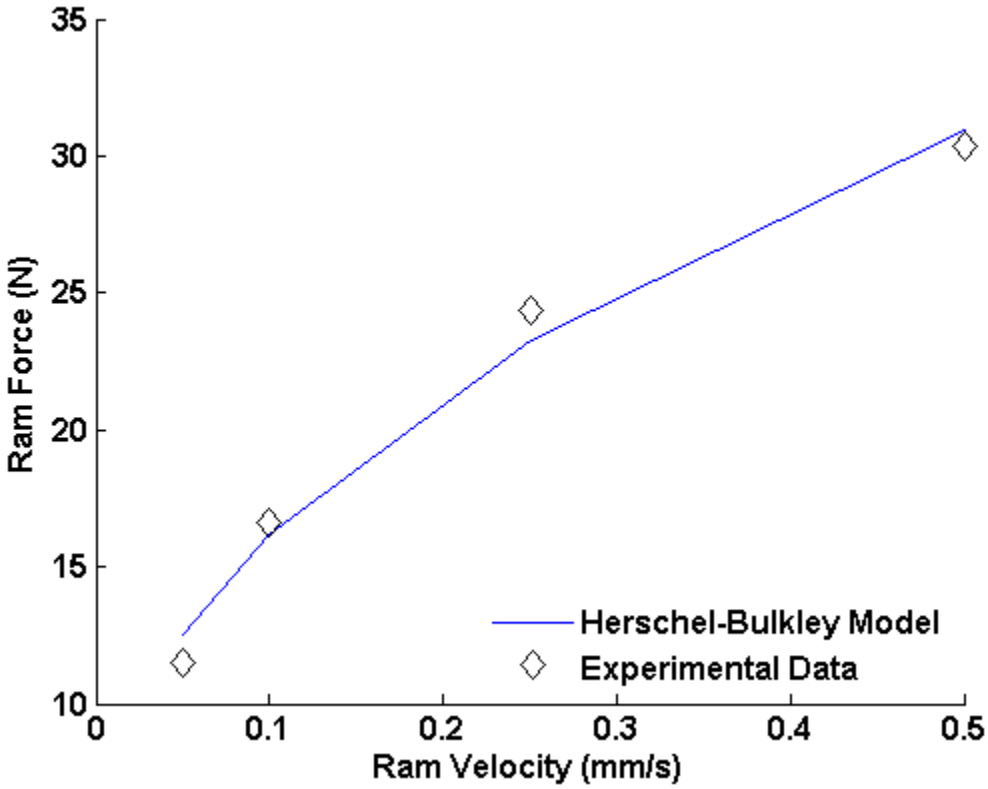

Fig. 5. Viscosity model test results.

Table 1. Material properties of alumina paste.

Viscosity model	
Consistency index $k\ (kg/m\cdot s)$	102.20
Power law index n	0.4626
Yield stress threshold $\tau_0\ (Pa)$	454.23
Critical shear rate $\gamma_c\ (1/s)$	10.042

4.2 Steady State

After determining the paste viscosity, tests are conducted using die 2 to experimentally verify the viscosity model. The viscosity model in equation (4) is used in the proposed mathematical model to predict the extrusion force. The comparison between validation experiment and analytical data is shown in Fig. 6.

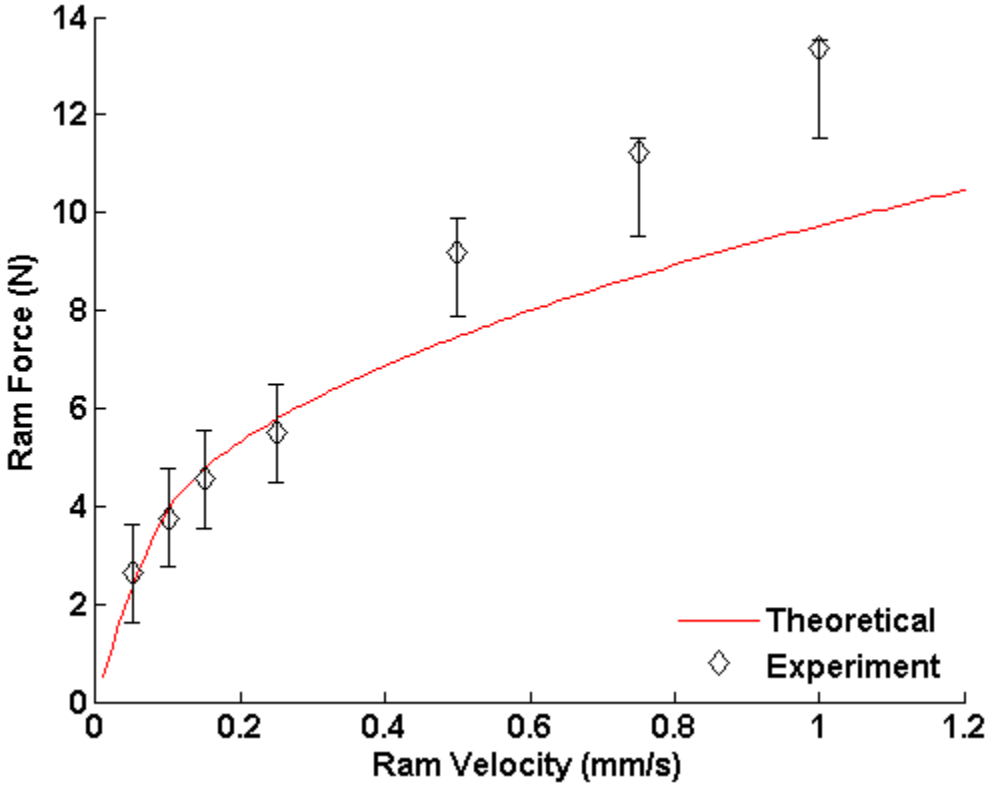

Fig. 6: Comparison of experimental and theoretical steady state extrusion forces using die 2.

It can be observed that good agreement is obtained between experiment and simulation results especially in low velocity area (see Table 2). The maximum absolute percent error is 27.1%. The difference in high velocity area may be caused by friction between barrel and plunger. Although the barrel is always well lubricated before each extrusion experiment, when the barrel is loaded with paste, the lubrication conditions may change. The error bars in Figure 6 are derived from a series of experiments with a variety of constant plunger velocities where paste was not extruded. The range of friction for each velocity was determined via the recorded ram forces in these experiments.

Table 2. Errors for experiments in Figure 6.

Ram Velocity (*mm/s*)	0.05	0.1	0.15	0.25	0.5	0.75	1
Error (%)|	11.3	4.65	4.57	4.94	18.7	22.5	27.1

4.3 Dynamic Response

To predict the extrusion force using the developed analytical model, the air volume fraction must be known. However, the air volume fraction in the paste is difficult to measure in practice and varies significantly between different batches of paste. To identify the air volume fraction, the extrusion process is given a set of constant velocities as shown in Figure 7. According to the dynamic model derived in Section 3.4, the dynamic response time constant is only a function of initial air layer thickness. Therefore, the time constant of first transient phase (in this case between 288 and 381 s) is be used to identify the air volume fraction. With the identified air volume fraction, the extrusion force dynamic response is calculated for different plunger velocities and compared with the experimental results, as shown in Fig. 7. In this case, according to the transient section between time 288 to 381 s, the initial air layer thickness is identified as 8.5 mm. The friction is assumed to be a constant 2 N based on the average of all of the friction data that was collected (not shown here). The friction varies tremendously from experiment to experiment. The results in Fig. 7 are plotted with a constant friction of 1.5 N. In this case the simulation shows much better correlation with the experiment.

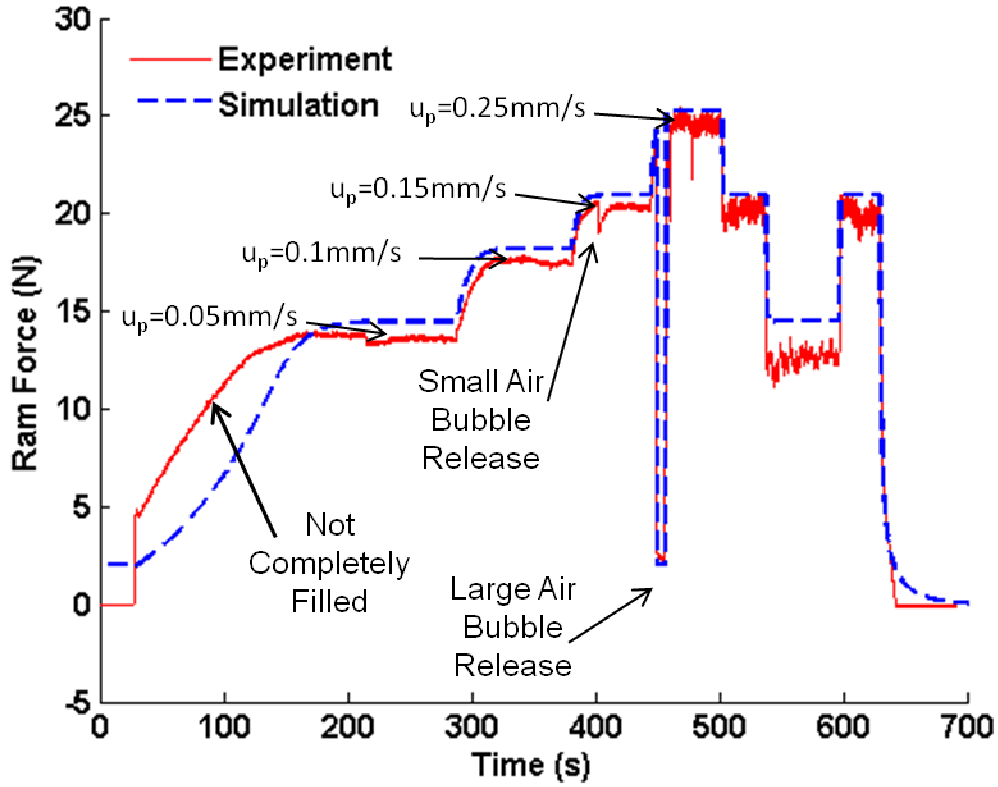

Fig. 7: Experimental and simulation dynamic extrusion responses with friction = 2 N.

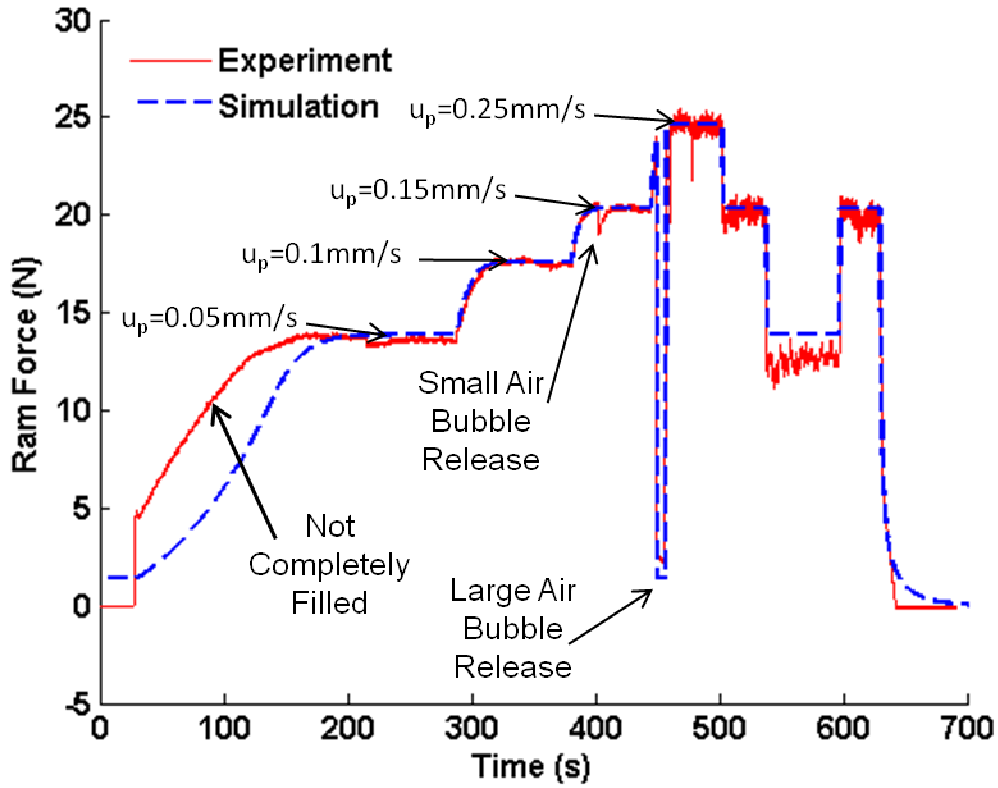

Fig. 8: Experimental and simulation dynamic extrusion responses with friction = 1.5 N.

It can be observed that

(1) Good agreement is obtained between the experimental and simulated steady state forces.

(2) Before the large air bubble release, good agreement is obtained between the experimental and simulated transient responses.

(3) After the large air bubble release, the transient response has a much smaller time constant, which means the compressibility is mainly caused by air trapped in paste.

(4) The difference of dynamic response at the beginning of extrusion may be due to the fact that the die is not completely filled by paste.

5. Summary and Conclusions

An analytical dynamic model was developed to describe the relationship between the ram velocity and extrusion force in the extrusion of aqueous–based ceramic materials. Based on the experimental and simulated results, the following conclusions can be drawn:

1. The mathematical model developed in this paper can be used to predict the steady state extrusion force and dynamic response in ram extrusion process of aqueous–based ceramic materials.

2. Since the paste viscosity is non–linear, the relationship between extrusion force and plunger velocity is also highly non–linear.

3. The large time constant of the dynamic response is mainly caused by the air trapped in the paste during both the paste preparation and loading procedures.

6. Acknowledgement

This project is supported by National Science Foundation (CMMI 0856419) and Center for Aerospace Manufacturing Technologies at Missouri University of Science and Technology.

7. References

[1] A. Bandyopadhyay, P. Panda, M. Agarwala, S. Danforth, and A. Safari, "Processing of Piezocomposites by Fused Deposition Technique," *Journal of the American Ceramic Society*, Vol. 80, No. 6, pp. 1366–1372, 2000.

[2] S. Crump, "Appartus and Method for Ceramic Three–Dimensional Objects," U.S.Patent No. 5121329, 1992.

[3] G. Hilmas, J. Lombardi, and R. Hoffman, "Advances in the Fabrication of Functional Graded Materials using Extrusion Freeform Fabrication," Functionally *Solid Freeform Fabrication Symposium*, Austin, TX, pp. 319–324, 1996.

[4] M. Cima, M. Oliveira, H. Wang, E. Sachs, and R. Holman, "Slurry–Based 3DP and Fine Ceramic Components," *Solid Freeform Fabrication Symposium*, Austin, TX, 2001.

[5] J. Kruth, P. Mercelis, L. Froyen, and M. Rombouts, "Binding Mechanisms in Selective Laser Sintering and Selective Laser Melting," *Solid Freeform Fabrication Symposium*, Austin, TX, 2004.

[6] M. Leu, E. Adamek, T. Huang, G. Hilmas, and F. Dogan, "Freeform Fabrication of Zirconium Diboride Parts Using Selective Laser Sintering," *Solid Freeform Fabrication Symposium*, Austin, TX , 2008.

[7] J. Stampfl, A. Cooper, R. Leitgeb, Y. Cheng, and F. Prinz, "Shape Deposition Manufacturing of Microscopic Ceramic and Metallic Parts Using Silicon Molds," U.S. Patent, No. 6242163, 2001.

[8] J. Cesarano III, R. Segalmen, and P. Calvert, "Robocasting Provides Moldless Fabrication from Slurry Deposition," *Ceramics Industry*, Vol. 148, pp. 94–102, 1998.

[9] G. He, D. Hirschfeld, J. Cesarano III, J. Stuecker, "Processing of Silicon Nitride–Tungsten Prototypes," *Ceramic Transactions*, Vol. 114, pp. 325–332, 2000.

[10] T. Huang, M. S. Mason, G. E. Hilmas, and M. C. Leu, "Freeze–Form Extrusion Fabrication of Ceramic Parts," *Virtual and Physical Prototyping*, Vol. 1, No. 2, pp. 93–100, 2006.

[11] M. S. Mason, T. Huang, R. G. Landers, M. C. Leu, and G. E. Hilmas, "Aqueous–based Extrusion of High Solids Loading Ceramic Pastes: Process Modeling and Control," *Journal of Materials Processing Technology*, Vol. 209, pp. 2946–2957, 2009.

[12] X. Zhao, R. G. Landers, and M. C. Leu, "Adaptive Extrusion Force Control of Freeze–form Extrusion Fabrication Processes," *ASME Journal of Manufacturing Science and Engineering*, Vol. 132, No. 6, 2010.

[13] J.J. Benbow, T.A. Lawson, E.W. Oxley and J. Bridgwater. "Prediction of Paste Extrusion Pressure," *American Ceramic Society Bulletin*, Vol.68, pp.1821–1824, 1989.

[14] M. Padmanabhan and M. Bhattacharya, "Analysis of Pressure Drop in Extruder Dies," *Journal of Food Science*, Vol. 54, pp. 709–713, 1989.

[15] T. Shepard, E. Nisaratanaporn and H.B. McShane, "Material Flow and Pressure Prediction when Extruding through Bridge Dies," *Zeitschrift fuer Metallkunde Materials Research and Advanced Techniques*, Vol.89, pp. 327–337, 1998.

[16] D.J. Horrobin and R.M. Nedderman, "Die Entry Pressure Drops in Paste Extrusion," *Chemical Engineering Science*, Vol. 53, No. 18, pp.3215–3225, 1998.

[17] U. Lang and W. Michaeli, "Development of a Mathematical Model for the Calculation of the Pressure Drop in Extrusion Dies," *Journal of Reinforced Plastics and Composites*, Vol. 17, pp. 1110–1118, 1998.

[18] Y. Y. Li and J. Bridgwater, "Prediction of Extrusion Pressure using an Artificial Neural Network," *Powder Technology*, Vol.108, No.1, pp. 65–73, 2000.

[19] W. Herschel and R. Bulkley. "Measurement of Consistency as Applied to Rubber Benzene Solutions," *ASTM Part II*, Vol. 26, No. 82: 621–629, 1926.